# LIDAR WAVEFORM CLASSIFICATION USING SELF-ORGANIZING MAP

**Piroska Zaletnyik**[1,2], Assistant Professor (Visiting Scholar)
**Sandor Laky**[1,2], Assistant Research Fellow (Visiting Scholar)
**Charles Toth**[1], Senior Research Scientist
[1]HAS-BME Research Group for Physical Geodesy and Geodynamics
Budapest University of Technology and Economics Budapest, H-1111, Hungary
zaletnyikp@gmail.com, laky.sandor@freemail.hu
[2] The Center for Mapping
The Ohio State University,
Columbus, OH 43210
toth@cfm.ohio-state.edu

## ABSTRACT

Most commercial LIDAR systems temporarily record the entire laser pulse echo signal, called full-waveform, as a function of time to extract the return pulses at data acquisition level in real-time; typically up to 4-5 returns. The new generation of airborne laser scanners, the full-waveform LiDAR systems, are not only able to digitize but can record the entire backscattered signal of each emitted pulse, which provides the possibility of further analyzing the waveform and, thus, obtaining additional information about the reflecting object and its geometric and physical characteristics. The LiDAR 3D point cloud and, subsequently, the derived DTM can be significantly improved by classifying the man-made objects and vegetation. Classification of the reflecting surfaces based on the statistical parameters of the backscattered waveform, however, is a non-trivial task.

The suburban test area used in this study offers a great diversity of surface types, including roof, pavement, grass, and trees. In this paper, the feasibility of classifying the reflecting surface based on waveform data using an unsupervised classification method, Kohonen's Self-Organizing Map (SOM) is investigated. The correlation between the shape of the waveforms, using various statistical parameters, such as standard deviation, skewness, kurtosis and amplitude, with the properties of the reflecting surface was investigated. These four statistical parameters were used as input to the SOM classification to separate vegetation (trees and grass) and non-vegetation surfaces. The ranges calculated from the center of mass of the waveform was used to separate the non-vegetation surface into pavement and roof categories.

## INTRODUCTION

Airborne LiDAR (also called as airborne laser scanning (ALS)) is used in many applications, such as digital elevation model (DEM) generation, 3D city modeling (Rottensteiner *et al*., 2005), metrology (Fidera *et al*., 2004), forest parameters estimation (Andersen *et al*., 2005), bridge and power line detection (Sithole and Vosselman, 2006), corridor, coastal mapping (Irish and Lillycrop, 1999) and also vertical object detection in aviation (Parrish, 2007).

The first commercially available airborne laser scanners provided only one backscattered echo per emitted pulse; later, the first and last echo (first and last pulse) of the backscattered signal could be measured (Shan and Toth, 2009). Current multi-echo or multiple pulse laser scanning systems are able to measure up to six pulses. Recently, a new generation of airborne laser scanners has appeared that are able to digitize and record the entire backscattered signal of each emitted pulse. They are generally called full-waveform (FW) LiDAR systems (Mallet and Bretar, 2009), and the waveform recording capability is either built-in or a user option.

The full-waveform LiDAR technology provides the possibility of further analyzing the waveform and, thus, obtaining additional information about reflecting objects and their geometric and physical characteristics. Obviously, the LiDAR 3D point cloud and derived DTM can be further improved by the waveform-based classification of man-made objects and vegetation.

There have been several studies addressing LiDAR data classification. As the first airborne laser scanners provided only 3D point clouds, the early classification algorithms used only LiDAR derived geometric primitives that were based on the geometric characteristics of a point relative to its neighborhood. Maas (1999) detected and modeled buildings using height texture measures and morphological filtering. Vögtle and Steinle (2003) used solely laser scanner derived digital elevation models for automated classification of 3D objects (trees, buildings) with fuzzy logic.

Later not only the first and last pulses but the intensity values of the backscattered signal were also provided to users. Tóvári and Vögtle (2004) used height textures, first/last pulse differences and intensity values to classify non-terrain objects. To improve the classification performance, others used not only LiDAR derived data, but other sources like aerial imagery (Brattberg and Tolt, 2008) or other available independent digital elevation model and aerial imagery (Charaniya *et al.*, 2004). Since the introduction of full-waveform LiDAR systems, there have been other possibilities to improve the efficiency of the classification of surface objects, as the entire waveform can be analyzed to derive additional information. Numerous studies are based on decomposing the waveform into sum of components or echoes to generate a denser and more accurate 3D point cloud (see Mallet and Bretar, 2009), modeling the waveforms with Gaussian (Wagner *et al.*, 2006), Generalized Gaussian or Lognormal function (Chauve *et al.*, 2007). Ducic *et al.*, (2006) decomposed the waveform into Gaussian components, and used this not only to improve the accuracy of the peak detection, but also to discriminate between vegetation and non-vegetation points using the parameters of the Gaussian functions, such as the amplitude and the standard deviation (pulse width). Mallet *et al.*, (2008) used the Generalized Gaussian model for classifying urban areas with one more parameter, the shape parameter of the Generalized Gaussian model, which allows simulating Gaussian, flattened or peaked pulses too. Both Ducic and Mallet used supervised classification methods; the first is based on the decision tree approach, while the second one uses Support Vector Machines.

In this paper, the feasibility study of classifying the reflecting surface is based on an unsupervised algorithm, the Kohonen's Self-Organizing Map (SOM). In our approach, the waveforms are first separated according to the number of echoes into two classes: one-echo or multiple-echo waveforms, and then the one-echo signals are treated as probability density functions, and the correlation of various statistical parameters, such as the maximum value of the intensity (amplitude), standard deviation (pulse width), skewness and the kurtosis with the properties of the reflecting surface are investigated. These parameters are subsequently used as input parameters for the SOM classification.

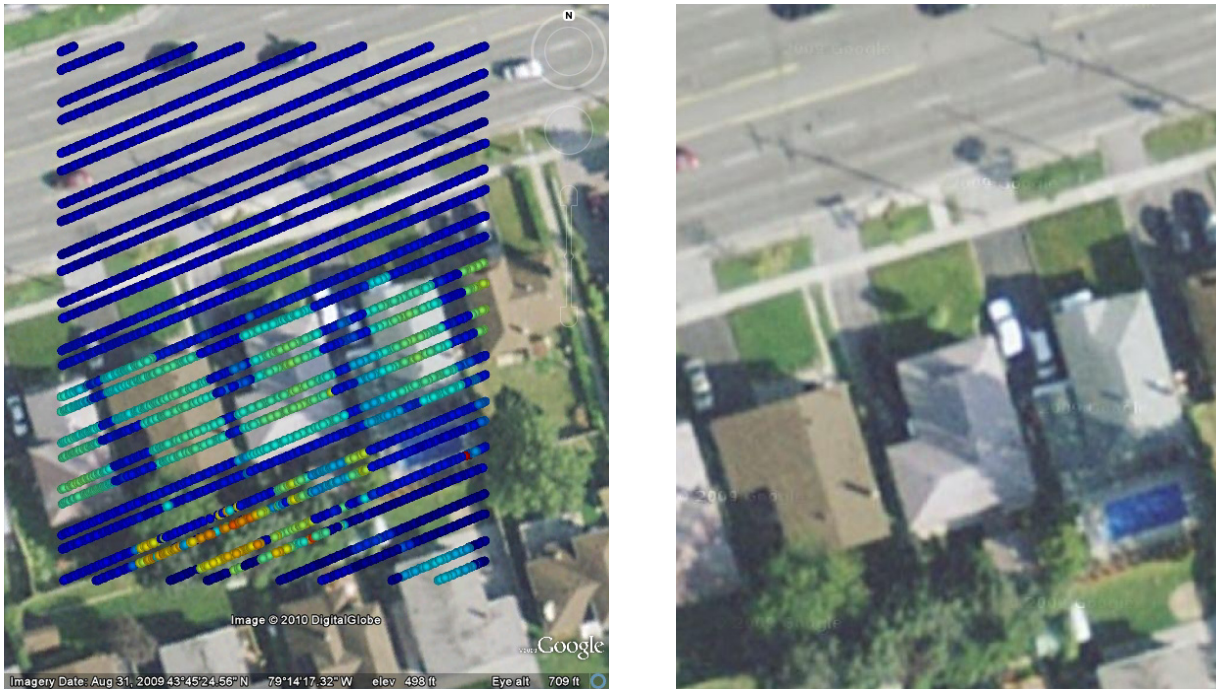


**Figure 1.** Sample area (image: Google Earth/Google Maps); points colored by height.

## SAMPLE FULL-WAVEFORM LIDAR DATA

The sample LiDAR dataset is from Ontario, collected over a residential area of Scarborough (Toronto) by an Optech ALTM 3100 full-waveform LiDAR system. The sampling interval of the digitizer is 1 nanosecond, and at the maximum acquisition and recording rate of 100 kHz the maximum return record length is 440 ns, acquired by two digitizers. The first unit starts acquiring data when the first return pulse is detected and continues until the signal is no longer present (i.e., below the threshold). The first segment is maximum 220 ns long. The second unit will not begin data acquisition until the signal rises above a certain threshold again. The captured signal is digitized by an 8-bit analog-to-digital (A/D) converter, giving a dynamic intensity range of 0-255. Note that each digitizer can cover targets extending over a range of 66 meters (Optech, 2005).

The measurement time of the Scarborough area dataset was around 16 seconds and the dataset contained more than 800,000 waveforms. For our classification study, we have chosen a smaller area (~50 x 65 m), with different types of surface coverage (grass, trees, pavement, roof and also a swimming pool), containing around 6,000 waveforms. In Figure 1, the left side shows the measured points in Google Earth, colored according to the heights of the points while the right side depicts our test area (from Google Maps). The distance between two adjacent points in a row is about 0.25 m, and the spacing between the rows is about 2-3.5 m.

To visually analyze the relation between the shapes of the waveforms and the objects where they were backscattered from, we developed a Google Maps-based application (PostgreSQL database backend, server-side scripts in PERL, client-side presentation using DHTML and JavaScript) to show the points and the corresponding waveforms on a satellite image background (see Figure 2). Picking a sample point, the program visualizes the corresponding waveform with the coordinates (latitude, longitude, elevation) and GPS time of the measurement. Selected waveforms can be saved, and custom SQL queries are also permitted.

Using this application different types of backscattered signals can be observed for trees, grass, pavement, roofs; some typical waveforms are illustrated in Figure 3.

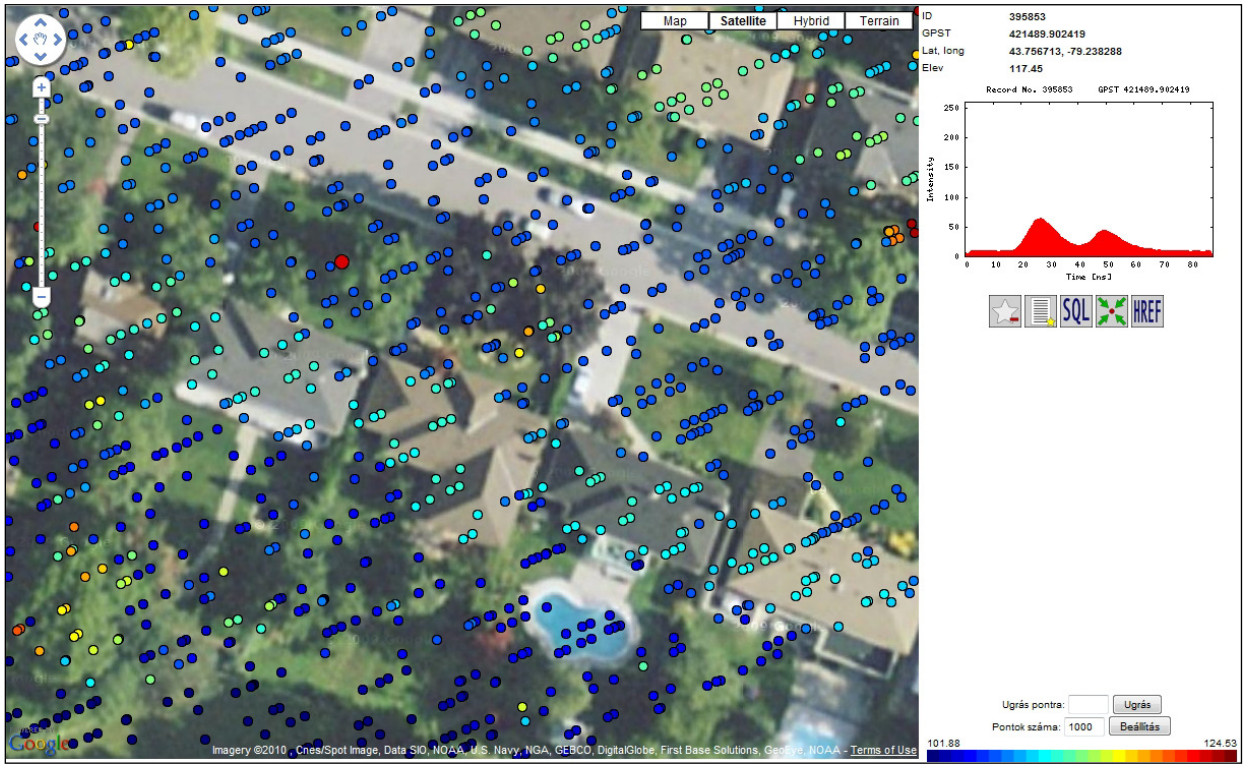


**Figure 2.** Web application to visualize/analyze the shape of the waveform and the corresponding surface coverage.

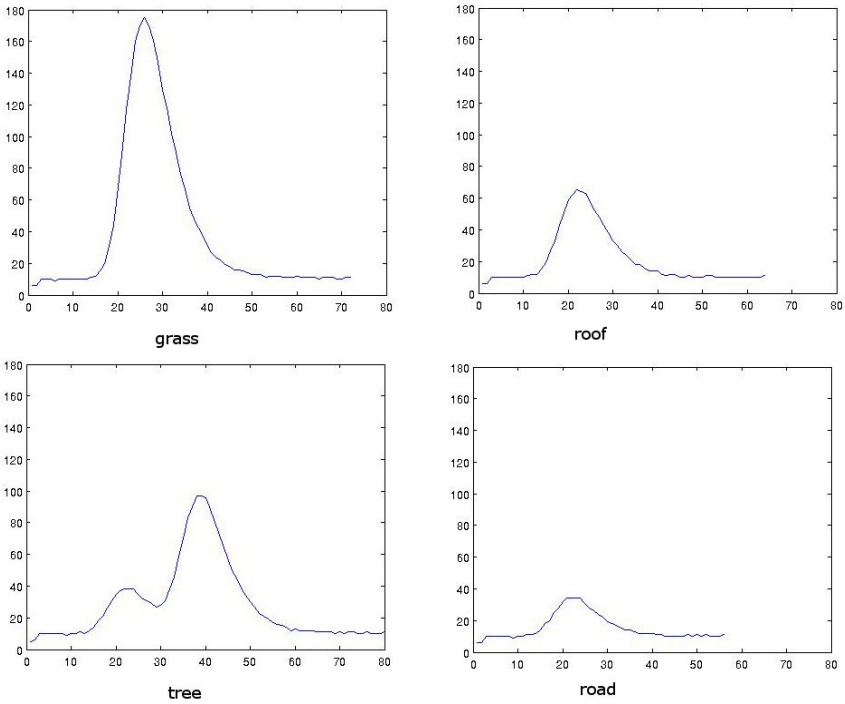


**Figure 3.** Typical waveform types according to different surfaces (x axis: time [ns], y axis: intensity), (Courtesy of Optech Incorporated).

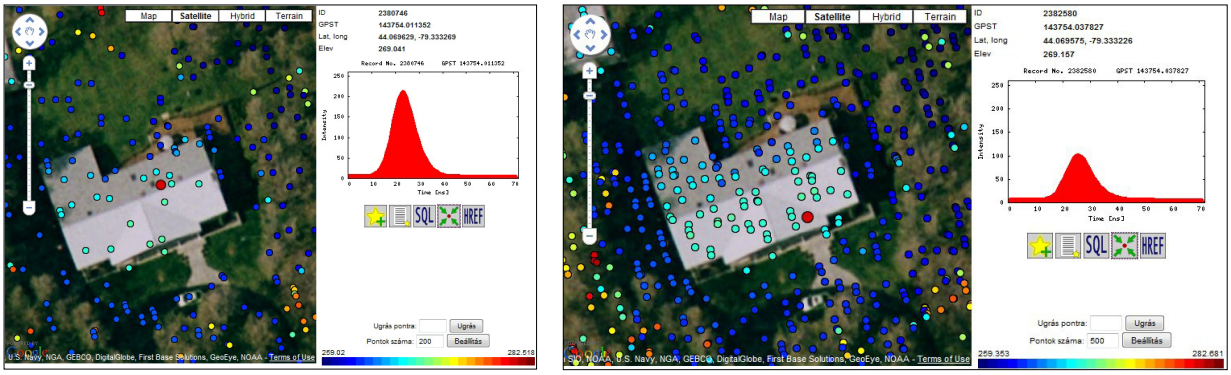


**Figure 4.** Varying waveforms according to different angle of incidents.

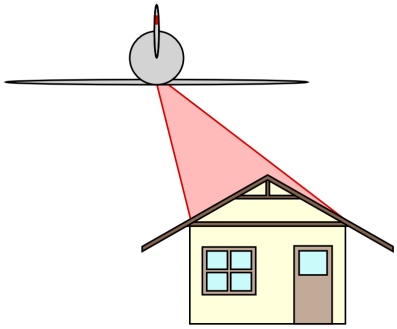

Using a different dataset, acquired in a forested area near Toronto, another important feature can be observed (see Figure 4). The ridge of the roof on the image is almost parallel to the direction of flight, so the angle of incidence in the two sides of the roof is significantly different. If we check the shapes of the waveforms from port and starboard sides, the amplitude (maximum intensity value) of the waveforms also change. This suggests correlation between the angles of incidence and the shape of the waveforms. This phenomenon could be more prevalent in metropolitan areas with skyscrapers or other high buildings, where pulses are backscattered from both the sides of the buildings and roofs.

## SHAPE PARAMETERS OF THE WAVEFORMS

From Figure 3, it can be seen that the backscattered waveforms have different shapes depending on the surface material. Thus, finding some typical characteristics of the waveforms, these parameters can be used for classification purposes. Obviously, one important parameter is the number of echoes. Here we first differentiate between one-echo and multiple-echo waveforms, and next we consider the significant differences among the one-echo waveforms.

In full-waveform processing, the waveform, in both cases, can generally be modeled with Gaussian functions (Wagner *et al.*, 2006), Chauve *et al.*, 2007)). A Gaussian function is a symmetrical, bell-shaped function, with two parameters, the mean and standard deviation. Looking at one-echo waveforms, it is easy to see that they are not uniform Gaussian shaped functions, as they can be asymmetric, peaked or flattened also. To distinguish between the different shapes, we can use statistical measures, which are generally used in some normality tests, such as skewness and kurtosis (see Figure 5).

In statistics, the skewness is a measure of the asymmetry of the probability density function. It is positive if the mass of the distribution is concentrated on the left side (see Figure 5b, green), negative if it is concentrated on the right (Figure 5b, red), and it is zero if the distribution is symmetric, like normal distribution (Figure 5b, blue). Skewness (s) is the standardized third central moment of the random variable *X*:

$$s = \frac{\mathrm{E}[(X-\mu)^3]}{\sigma^3},$$

where μ is the mean, and σ is the standard deviation.

Kurtosis is a measure of the peakedness or flattening of a probability density function. The normal distribution has kurtosis of 3. If the kurtosis is higher than 3 the distribution is more peaked, if it is less than 3, it is more flattened than the normal distribution. Kurtosis (κ) is the standardized fourth central moment of the random variable X:

$$\kappa = \frac{\mathrm{E}[(X-\mu)^4]}{\sigma^4},$$

where μ is the mean, and σ is the standard deviation. The excess kurtosis is commonly used instead of the kurtosis, which is equal to kurtosis minus 3 (to make the kurtosis of the normal distribution equal to zero).

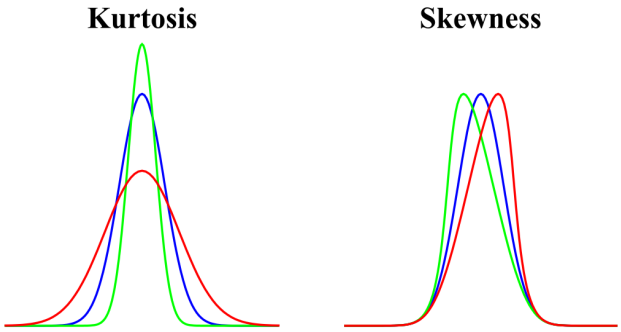


**Figure 5.** Skewness and kurtosis.

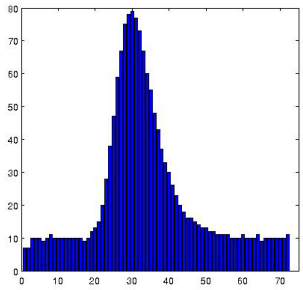


**Figure 6.** "Histogram" of a waveform.

Treating the one-echo waveforms as probability density functions (see Figure 6.), the standard deviation, skewness and kurtosis can be calculated as shape parameters. The amplitude (maximum intensity value) of the waveforms is also an important parameter for the classification (Tóvári and Vögtle, 2004).

As skewness and kurtosis has a meaning only for unimodal distribution (comparing the shape to the normal distribution), first the waveforms have to be separated according to the number of peaks. For this step, a pulse detection method to count the number of the pulses in waveforms was used. The histograms of the calculated parameters for the one-echo waveforms are shown in Figure 7.

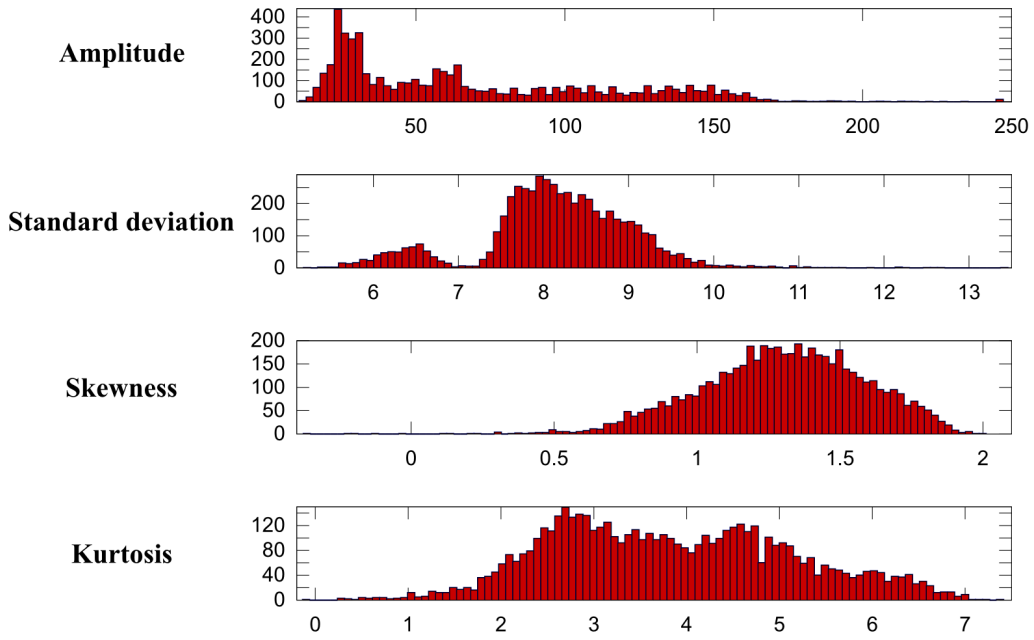


**Figure 7.** Shape parameters of the Scarborough test area.

## CLASSIFICATION ACCORDING TO THE WAVEFORMS SHAPES

As shown in Figure 3, the shapes of the waveforms can be very different, thus, it is assumed that there is a correlation between the shape of waveforms and the backscattering surface material. Therefore, objective is to classify the surface coverage of the test area, shown in Figure 1, into 4 classes: grass, trees, pavement and roof.

Classification algorithms can be divided into two main groups, supervised and unsupervised classification. In the supervised classification, a training and a test dataset are used; where the output class types belonging to the input are known. In machine learning, unsupervised classification is also called clustering or cluster analysis, where the set of observations are divided into subsets (called clusters), so that observations in the same cluster are similar in some sense. The advantage of this classification is that there is no need to have a priori knowledge of the class types belonging to a training or test dataset. Clustering is a common technique for statistical data analysis and used in many fields. There are different methods like hierarchical clustering, K-means or Self-Organizing Map (SOM), an artificial neural network type clustering, etc.

In this study, we used the SOM clustering, which was first described as an artificial neural network model by Teuvo Kohonen (Kohonen 1990), and therefore, the model is also called Kohonen map.

The SOM represents the result of a vector quantization algorithm that places a number of reference or codebook vectors into a high dimensional input data space to approximate its data sets in an ordered fashion. A typical application of SOM is in the analysis of complex vectorial data where the data elements may even be related to each other in a highly nonlinear fashion. The process, in which the SOM is formed, is an unsupervised learning process (Kohonen *et al.*, 1996).

The SOM defines a mapping from the input data space $\mathcal{R}^n$ onto a regular two dimensional array of nodes. With every node *i*, a parametric reference vector $m_i \in \mathcal{R}^n$ is associated. The lattice type of the array can be defined as rectangular or hexagonal. An input vector $x \in \mathcal{R}^n$ is compared with the $m_i$ and the best match is defined as response to the input, and thus, is mapped onto this location. The SOM is a nonlinear projection of the probability density function of the high dimensional input data onto the two dimensional domain.

For the SOM classification, the SOM_PAK program package, freely available for scientific purposes, prepared by the SOM programming team of the Helsinki University of Technology (Kohonen *et al.*, 1996), was used.

## Separation of one-echo and multiple-echo waveforms

The basic peak detection method is based on the zero crossings of the first derivative on the thresholded version of the waveform (Chauve *et al.,* 2007). In our method, first a low pass filter to avoid the multiple close peaks caused by noise was used, and then the peaks were detected with the method referenced above. In the Scarborough suburban test area, 93.4% of the waveforms had one peak and 6.6% had two or more peaks (389 from the 5,877 waveforms). Most of the multiple-echo waveforms were backscattered from trees and some from non-vegetation areas, mainly from the edges of the buildings, which can be seen well in Figure 8a (compare it to Figure 1). Using the different densities of these points (in vegetation areas the multiple-echo points are more frequent and dense), the multiple-echo waveforms were separated into two classes (see Figure 8b): vegetation (309 waveforms) and non-vegetation (80 waveforms).

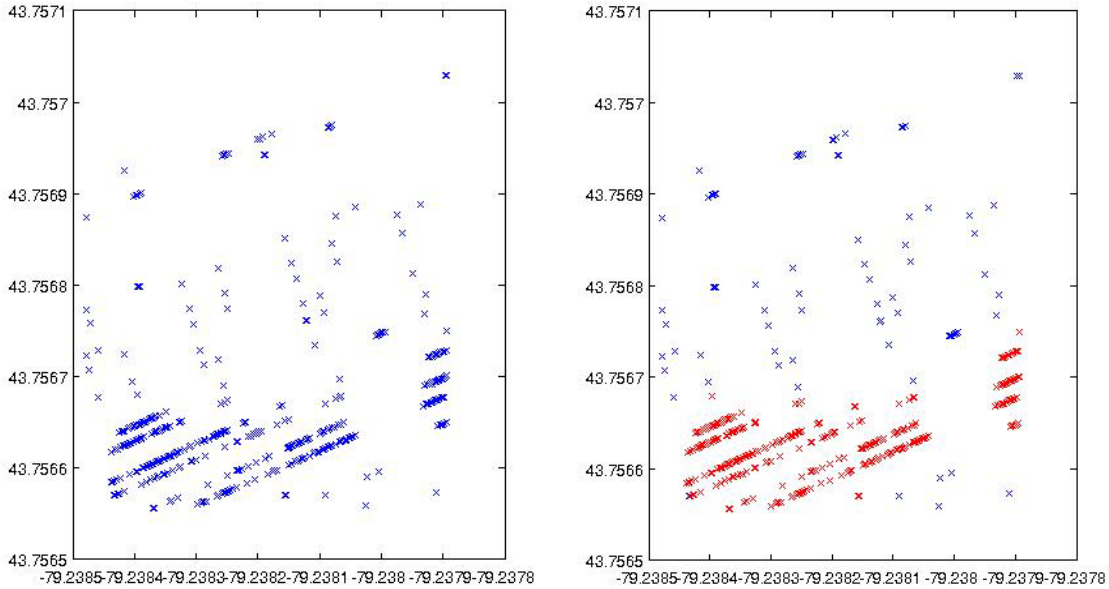


(a) (b)

**Figure 8.** a) Multiple-echo waveforms, b) Vegetation (red) and non-vegetation (blue) multiple-echo waveforms.

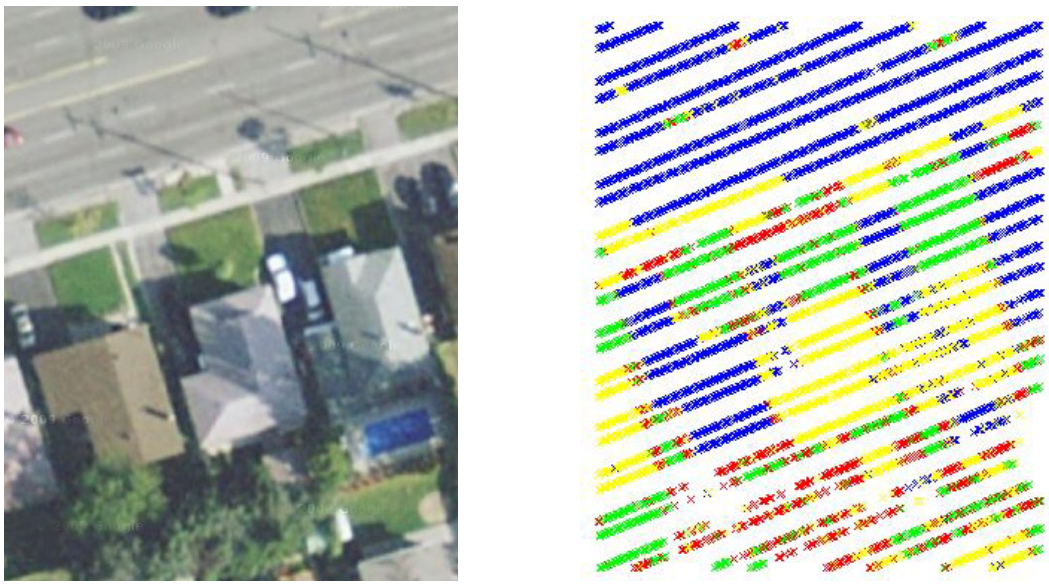

**Figure 9.** Initial classification results according to the waveforms shape.

## Classification of one-echo waveforms according to their shapes

For the classification of the one-echo waveforms (5,488 waveforms), the above mentioned four shape parameters were used in the SOM clustering of hexagonal lattice type and 2x2 nodes. The initial result showed that there is a high correlation between the shape of the waveforms and the backscattering surface, as shown in Figure 9. Note that grass and trees can be quite well separated from the pavement and roofs. There are four main buildings in this area; three can be well separated according to the waveform shapes from pavement, but one is categorized as pavement. In the aerial image, it can be noticed that the roof material of this building is also different from the others.

While these results are promising, the open question is: can it be improved? We tried different types of SOM, using different topology types (rectangular, hexagonal), using more classes first and then group the categories later, different neighborhood functions (step function, Gaussian function), and then tried to rescale, standardize the input but the results did not improve considerably. In addition, we tried to use the slope of the surface as a fifth input parameter, as the roofs normally have higher slopes then pavement. However, it did not work in this case, as after calculating the slopes, it became evident that the misclassified roof is a flat roof (compared to the others), and has about the same slope as the pavement (see Figure 10). This means that the angle of incident has a very important role in forming the shape of the waveform. But it also means that another method is needed to further improve the classification performance.

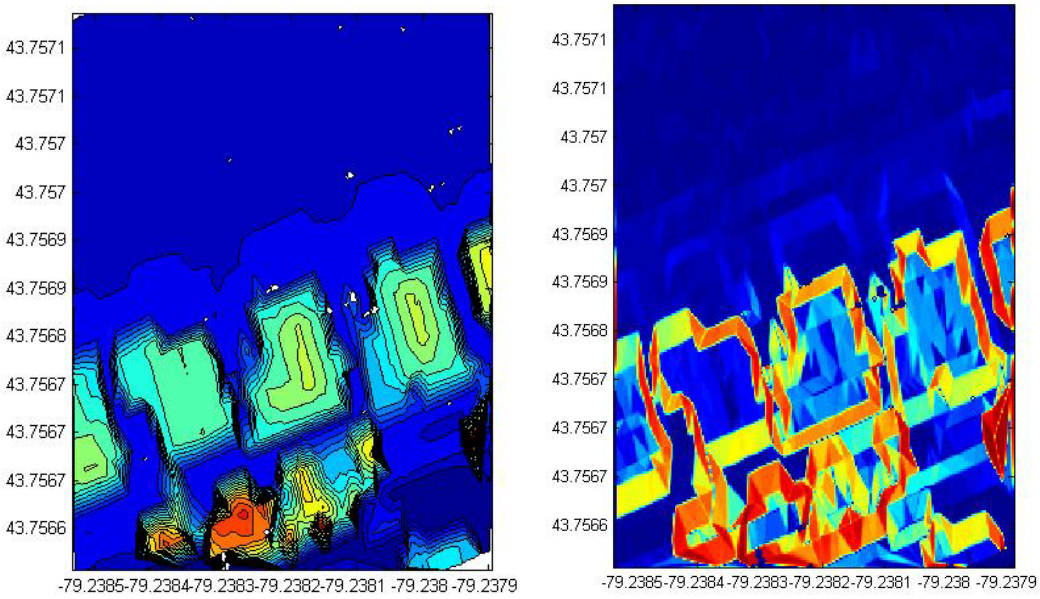


(a) (b)

Figure 10. a) Digital Surface Model (DSM) of the area, b) slope categories.

In summary, vegetation and non-vegetation areas can be well separated based only on the waveforms parameters. The efficiency of the classification can be increased if it is done in two steps. First, we separate non-vegetation areas (man-made objects) from vegetation, and then classify vegetation as trees and grass, and non-vegetation as pavement and roof. The waveforms of trees and grass can be separated rather well in this way, while between pavement and roof, there is always a chance for misclassification.

Our primary goal in this effort was to do the classification based on only the waveforms. One motivation is that the classification can be applied real-time, which could lead to implementing more efficient data acquisition and processing performance. For example, the usual method of separating buildings (roofs) and pavement would require calculating the height of each point above the terrain (which is approximated by the minimum elevation in a given radius around the given point), which, in turn, would require the calculation of the coordinates of every point, which can be only done using navigation information. To avoid the need for this calculation, given the relatively smooth flight conditions during scanning, the difference of elevations can be substituted by the difference of ranges. The range from the scanner to the backscattering point can be calculated by using only waveform data (approximating the time of the echo by the time corresponding to the center of mass of the waveform, which statistically means the expected value of the

probability density function plus the starting time of the return waveform). In addition, this is also influenced by the scan angle. However, examining a relatively small area, the differences between the actual pulse range and the highest range (lowest elevation) can be a good approximation of the height above the terrain. Once, these approximate ranges calculated and examining the successive waveforms in the rows (80 previous and 80 subsequent waveforms were used, which correspond to approximately 2x20 m of distance), the pulse range difference between the highest range (the point with the smallest elevation) and the range of the actual point was calculated. In this way, low areas and locally high areas can be separated well, as shown in Figure 11.

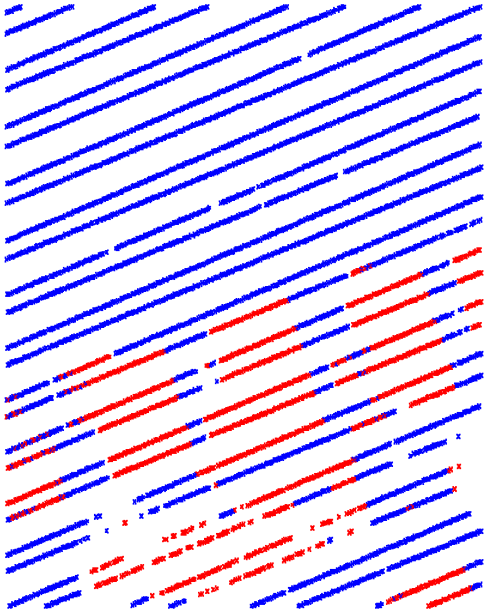

**Figure 11.** Local range differences.

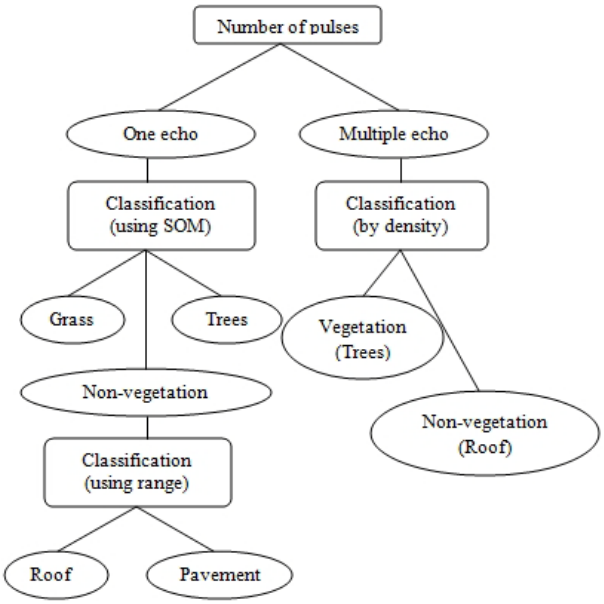


**Figure 12.** Classification algorithm.

After separating the one-echo and multiple-echo waveforms, a two step classification was used on the one-echo waveforms. First grass, trees and non-vegetation areas were separated according to the afore mentioned waveform shape parameters, and then the non-vegetation areas were separated into pavement and roof, using the ranges of the pulses, see Figure 12.

In Figures 13 and 14, the histograms of the waveform parameters are shown for the four classes. It can be seen that the most important parameter is the amplitude, though this parameter alone is not enough for unsupervised classification, but together with the other parameters, and also with the range based separation, the waveforms can be classified efficiently.

For visualization, the results of the four classes were interpolated to a grid, see Figure 15. The results can be further improved using filtering, to avoid unique misclassified points in the area. For this, we used the mode of the class value in a small environment (half a meter radius). The results after the filtering are shown in Figure 16. Unfortunately, in one direction the resolution is limited by the spacing between the rows (about 2-3.5 m); that is the reason of the blocky appearance of the resulting map.

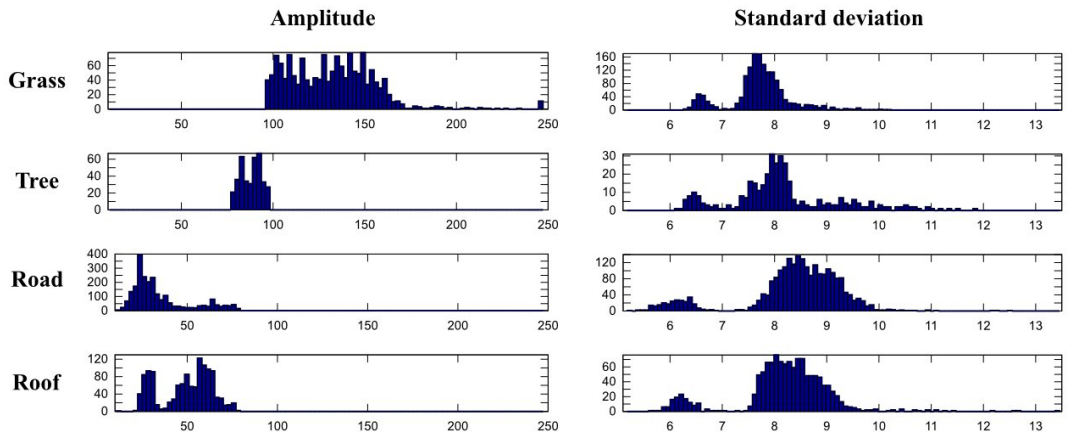


**Figure 13.** Histograms of amplitude and standard deviation for the four classes.

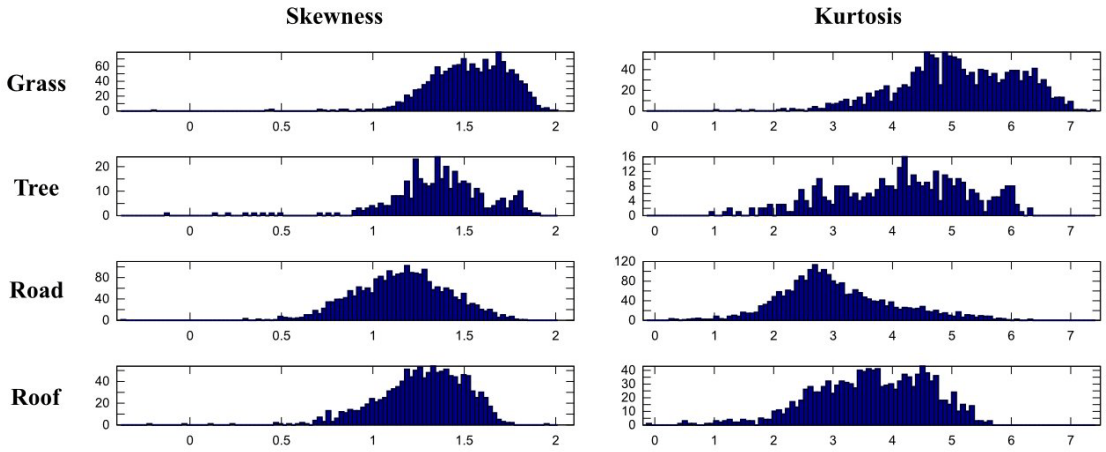


**Figure 14.** Histograms of the skewness and kurtosis for the four classes.

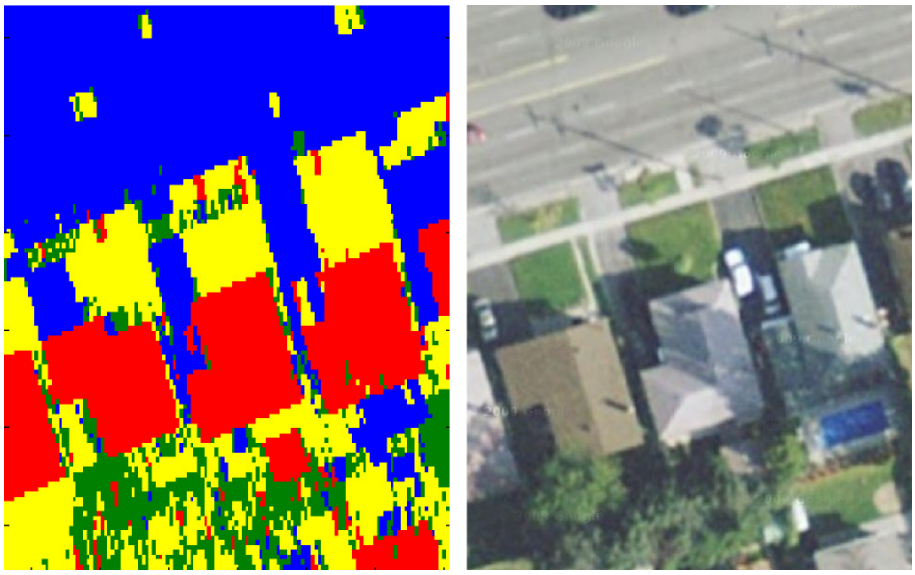

**Figure 15.** Result of the classification before filtering.

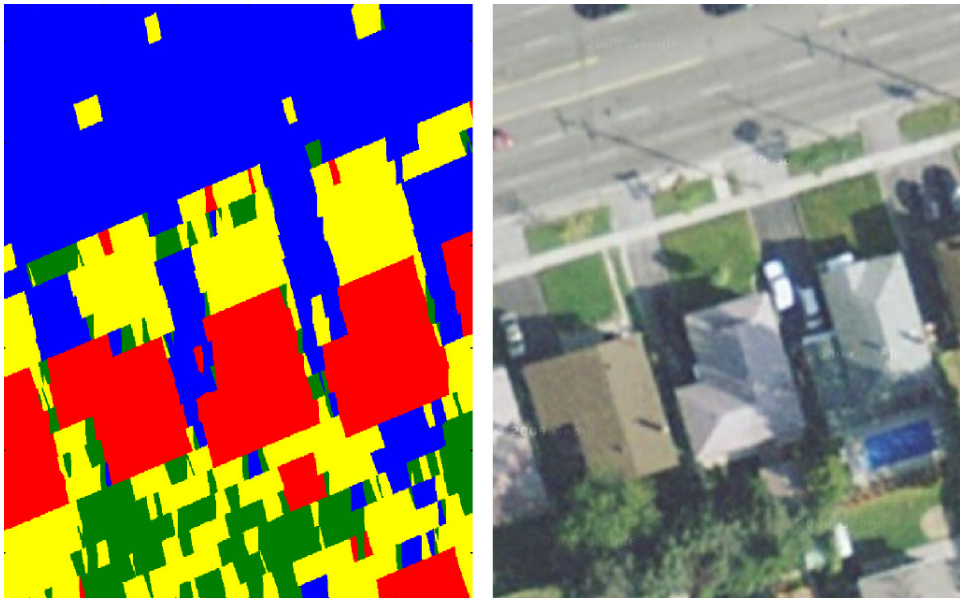

**Figure 16**. The final result of the classification.

## SUMMARY

In this study, a method for full-waveform LiDAR data classification was developed, based on using only waveform characteristics, to assess the efficiency of the waveform data for classification purposes.

To visually analyze the relation between the waveforms and backscattering surface, a Google Maps-based application was developed. Using this application, different types of backscattered signals were observed for trees, grass, pavement, roofs from a suburban sample dataset. It was identified that there is a correlation between the shape of the waveforms and the backscattering material, which can be exploited for classification purposes, and thus, the standard LiDAR derived 3D point cloud can be significantly improved. It was also evidenced that there is correlation between the shapes of the waveforms and the angle of incidence.

In the proposed method, waveforms were separated into one- and multiple-echo waveforms, and statistical parameters of the one-echo waveforms, such as the expected value, standard deviation, skewness, kurtosis and amplitude were calculated. The last four parameters were used as input parameters for an unsupervised classification method, the SOM classification, to divide the observation set into three subsets, corresponding to trees, grass and non-vegetation areas. The classification was enhanced by separating the non-vegetation areas into pavement and roof, using the expected value with the starting time of the backscattered waveforms. Finally, by filtering the classified points (using the mode of the class values in a small environment), the classification was further improved by eliminating unique misclassified points.

Visual comparison of the results of the classification with aerial imagery shows that full-waveform LiDAR data can be used not only to generate a denser and more accurate 3D point cloud, but analyzing the shape of the waveforms provides a very efficient way to separate the different types of surfaces such as trees, grass, pavement and roofs in urban areas.

## ACKNOWLEDGEMENT

The authors thank to Optech Incorporated for the data provided for this research.

The first author wish to thank to The Thomas Cholnoky Foundation for the support of her visit at The Center for Mapping at The Ohio State University, during the time-period this work has been accomplished.

## REFERENCES


Andersen, H.-E., McGaughey, R., Reutebuch, S., 2005. Estimating forest canopy fuel parameters using LIDAR data. Remote Sensing of Environment 94 (6), 441-449.

Brattberg, O.; Tolt, G., 2008. Terrain Classification Using Airborne LiDAR Data and Aerial Imagery, The International Archives of the Photogrammetry, Remote Sensing and Spatial Information Sciences. Vol. XXXVII. Part B3b. Beijing 2008, pp. 261-266.

Charaniya, A.; Manduchi, R; Lodha, S., 2004. Supervised Paramteric Classification of LiDAR Data, IEEE Workshop on Real Time 3D Sensor and Their Use, Washington DC, June 2004, 8 pages

Chauve, A., Mallet, C., Bretar, F., Durrieu, S., Pierrot-Deseilligny, M., Puech, W., 2007. Processing full-waveform LiDAR data: Modelling raw signals. International Archives of Photogrammetry, Remote Sensing and Spatial Information Sciences 36 (Part 3/W52), pp. 102-107.

Ducic, V., Hollaus, M., Ullrich, A., Wagner, W., Melzer, T., 2006. 3D vegetation mapping and classification using full-waveform laser scanning. In: Proc. Workshop on 3D Remote Sensing in Forestry. EARSeL/ISPRS, Vienna, Austria, 1415 February 2006, pp. 211-217.

Fidera, A., Chapman, M., Hong, J., 2004. Terrestrial LiDAR for industrial metrology applications: Modelling, enhancement and reconstruction. International Archives of Photogrammetry, Remote Sensing and Spatial Information Sciences 35 (Part B5), pp. 880-883.

Irish, J., Lillycrop, W., 1999. Scanning laser mapping of the coastal zone: The SHOALS system. ISPRS Journal of Photogrammetry & Remote Sensing 54 (2_3), pp. 123-129.

Kohonen, T., 1990. The Self-Organizing Map, Proc. IEEE, Vol. 78., No. 9., pp. 1464-1480.

Kohonen, T., Hynninen, J., Kangas, J., Laaksonen, J. 1996. SOM_PAK, The Self-Organizing Map Program Package, Technical Report A31, Helsinki University of Technology, Laboratory of Computer and Information Science, FIN-02150 Espoo, Finland, 27 pages

Maas, H.G., 1999. Fast determination of parametric house models from dense airborne laserscanner data. In: The International Archives of the Photogrammetry and Remote Sensing, Bangkok, Thailand, Vol. XXXII, 2/W1, pp. 1–6.

Mallet, C., Soergel, U., Bretar, F., 2008. Analysis of full-waveform lidar data for an accurate classification of urban areas. International Archives of Photogrammetry, Remote Sensing and Spatial Information Sciences 37 (Part 3A), pp. 85-92.

Mallet, C., Bretar, F., 2009. Full-waveform topographic LiDAR: State-of-the-art, ISPRS Journal of Photogrammetry and Remote Sensing, Volume 64, Issue 1, pp. 1-16.

Optech Incorporated, 2005. Airborne Laser Terrain Mapper (ALTM) Waveform Digitizer Manual, Optech Incorporated, Toronto, Ontario, Canada, Document No. 0028443/Rev A.5

Parrish, C. E., 2007. Exploiting full-waveform LiDAR data and multiresolution wavelet analysis for vertical object detection and recognition, Geoscience and Remote Sensing Symposium, 2007. IGARSS 2007. IEEE International, pp. 2499-2502.

Rottensteiner, F.; Trinder, J.; Clode, S., 2005. Data acquisition for 3D city models from LIDAR extracting buildings and roads, Geoscience and Remote Sensing Symposium, 2005. IGARSS '05. Proceedings. 2005 IEEE International, Volume 1, pp. 521-524.

Sithole, G., Vosselman, G., 2006. Bridge detection in airborne laser scanner data. ISPRS Journal of Photogrammetry & Remote Sensing 61 (1), pp. 33-46.

Shan, J., and Toth, C. K., 2009. Topographic Laser Ranging and Scanning—Principles and Processing, CRC Press Taylor & Francis, London, 590 pages

Tóvári, D., Vögtle, T., 2004. Object Classification in Laserscanning Data. In: International Archives of Photogrammetry, Remote Sensing and Spatial Information Sciences, Freiburg, Germany, Vol. XXXVI, Part 8/W2, pp. 45-49.

Vögtle, T., Steinle, E., 2003. On the quality of object classification and automated building modeling based on laserscanning data. In: The International Archives of the Photogrammetry, Remote Sensing and Spatial Information Sciences, Dresden, Germany, Vol. XXXIV, 3/W13, pp. 149–155.

Wagner, W., Ullrich, A., Ducic, V., Melzer, T. and Studnicka, N., 2006. Gaussian decomposition and calibration of a novel small-footprint full-waveform digitising airborne laser scanner. ISPRS Journal of Photogrammetry & Remote Sensing 60(2), pp. 100–112.